A Novel Zero/Reduced Common-Mode Voltage Modulation Scheme for a Dual Three-Phase Motor Drive System in Full Modulation Span

Yang Huang, *Student Member, IEEE*, Jared Walden, *Student Member, IEEE*, Ximu Zhang, Yu Yan, *Student Member, IEEE*, Hua Bai, *Senior Member, IEEE*, Fanning Jin, *Student Member, IEEE*, and Bing Cheng, *Member, IEEE*

***Abstract*—Common-mode voltage (CMV) is one of the major concerns in modern motor drive systems using pulsewidth modulation (PWM) controls. To alleviate the CMV issue, a series of different PWM methods have been proposed. However, due to the physical limits of the three-phase structure, none of those reduced-CMV PWMs (RCMV-PWMs) can fully eliminate the CMV. As the motor phases have been extended to even numbers, such as six phases, opportunities to eliminate the CMV by a proper modulation scheme emerge. This article proposes a new modulation method to fully eliminate or reduce the CMV for the full modulation span of a dual-three-phase motor drive system, thereby helping to shrink the CM filter. Mathematical models are built indicating its effectiveness of eliminating the CMV in the linearity range of the modulation index and reducing the CMV in the overmodulation range. Simulation results along with experiments implemented on field-programmable gate array controlled dual inverters validated the effectiveness of the proposed control algorithm.**

***Index Terms*—Common-mode voltage (CMV), dual three-phase motor, space vector modulation (SVM).**

NOMENCLATURE

CMV	Common-mode voltage.
CMC	Common-mode current.
DM	Differential-mode.
RCMVM	Reduced common-mode voltage modulation.
ZCMVM	Zero common-mode voltage modulation.
ZRCMVM	Zero/reduced common-mode voltage modulation.
DTM	Dual three-phase motor.
MI	Modulation index.
CSPWM	Conventional sinusoidal PWM.
CSVM	Conventional space vector modulation.
AZSPWM	Active zero-state PWM.
$D_{a,b,c,d,e,f}$	Duty cycle of phase A, B, C, D, E, F.
$D_{d1,2,e1,2,f1,2}$	Split duty cycle of phase D, E, F.
$D_{\mathrm{on/off}}$	ON/OFF time duty cycle.
LISN	Line impedance stabilization network.

Manuscript received August 17, 2021; revised October 23, 2021 and November 29, 2021; accepted December 31, 2021. Date of publication January 4, 2022; date of current version February 18, 2022. This work was supported by Mercedes-Benz Research and Development North America. This work made use of the Engineering Research Center Shared Facilities supported in part by the Engineering Research Center Program of the National Science Foundation and DOE under NSF Award EEC-1041877 and in part by the CURENT Industry Partnership Program. Recommended for publication by Associate Editor D.-C. Lee. *(Corresponding author: Hua Bai.)*

Yang Huang, Jared Walden, Ximu Zhang, Yu Yan, and Hua Bai are with the Department of Electrical Engineering and Computer Science, University of Tennessee, Knoxville, TN 37996 USA (e-mail: yhuang65@vols.utk.edu; jwalde12@vols.utk.edu; xzhan134@vols.utk.edu; yyan15@vols.utk.edu; kevinbai@icloud.com).

Fanning Jin and Bing Cheng are with Mercedes Benz Research/Development North America, Redford, MI 48239 USA (e-mail: fanning.jin@daimler.com; bing.cheng@daimler.com).

Color versions of one or more figures in this article are available at https://doi.org/10.1109/TPEL.2022.3140261.

Digital Object Identifier 10.1109/TPEL.2022.3140261

I. INTRODUCTION

SPACE vector modulation (SVM) is widely adopted in the three-phase motor drive system. With the switching frequency increasing particularly when using wide-bandgap (WBG) devices, the common-mode voltage (CMV) becomes the major drawback. As shown in Fig. 1, traditional center-aligned pulsewidth modulation (PWM) generates CMV varying between $\pm V_{\mathrm{dc}}/6$ or $\pm V_{\mathrm{dc}}/2$ in a three-phase two-level inverter. Equation (1) defines the CMV in a three-phase system, where V_{ao}, V_{bo}, V_{co} denote the voltage between the phase leg output and the dc-link middle point. These values show the CMV (V_{CM}) can never be zero, which subsequently yields a large CM choke for the sake of complying with CM standards, such as CISPR 25 in electric vehicles (EVs). Both cost and weight are then added to the inverter system. In the past decades, motors with a phase number higher than three, such as dual-three-phase motors (DTMs), have drawn attention of EV industry as the three-phase system cannot eliminate the CMV [1], [2]. Fig. 2 shows one type of the DTM driven by dual inverters, where the neutral points for two sets of three-phase windings are separated with the winding angle difference of 30°. Such motors show advantages over the conventional three-phase motors in terms of reliability; power density; fault tolerance; torque pulsations; and current stress, thereby becoming popular in safety-critical and high-power applications [3]–[8].

Compared with the DTM drive with a single neutral point [9], [10], a neutral-point-separated DTM provides more flexibility on the control for each set of winding, therefore reducing the control complexity. In terms of the CMV performance, (2) formulates the CMV for a DTM. As the phase count is an even number, by imposing $V_{\mathrm{dc}}/2$ to one phase and $-V_{\mathrm{dc}}/2$ to the other, there

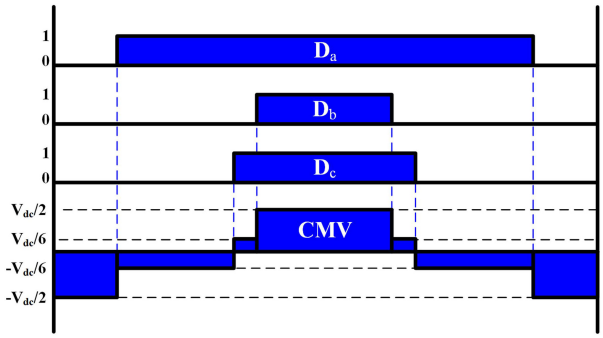

Fig. 1. Three-phase center-aligned modulation and the corresponding.

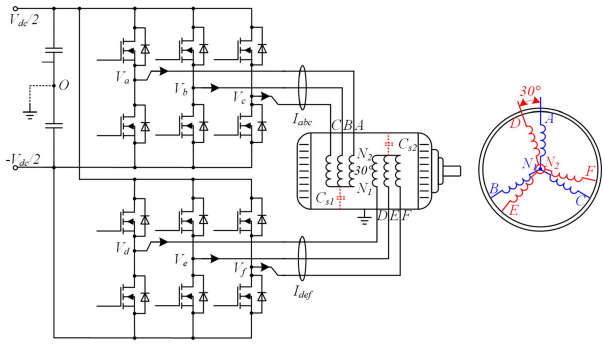

Fig. 2. Drive system for a DTM.

exists the possibility to eliminate the CMV [11], [12]

$$V_{\mathrm{CM}} = (V_{ao} + V_{bo} + V_{co})/3 \tag{1}$$

$$V_{\mathrm{CM}} = (V_{ao} + V_{bo} + V_{co} + V_{do} + V_{eo} + V_{fo})/6. \tag{2}$$

For safety concern, the motor case and the middle point of the dc-link are typically grounded to the chassis [13]. The parasitic capacitor (*Cs*) across the winding neutral and chassis will provide the path for the CM current (CMC), induce shaft voltage, and bearing current [14]–[17]. This will cause insulation failure, greatly shorten the motor lifespan, and cause significant EMI problems. To make the situation worse, WBG devices such as SiC MOSFETs are more commonly being used in motor drive systems. Their superior switching performance results in high CMV by introducing a high switching frequency (*fs*) and high *dv/dt* [3], [18].

In the six-phase modulation, we can take the conventional sinusoidal PWM (CSPWM) as an example. The gate signals of all switches are still center-aligned, as shown in Fig. 3(left). Here, $D_{a\text{-}f}$ denotes the duty cycle of each phase, and the overall CMV exhibits a seven-level profile with the peak value equal to $\pm V_{\mathrm{dc}}/2$. Given each switch-ON action results in the step of $V_{\mathrm{dc}}/2$ at the corresponding phase-leg output and a switch-OFF action generates $-V_{\mathrm{dc}}/2$, every switching action at any phase results in a step change of the CMV. For a conventional PWM control, in one switching period switching actions of two phases cannot happen simultaneously, which still yields a large CMV. By shifting or splitting PWM signals to create switch-ON/OFF pairs among phases while keeping the duty cycle of phases unchanged, CMV can be eliminated as the $\pm V_{\mathrm{dc}}/2$ step-changes at different phases offset each other. This approach is named zero

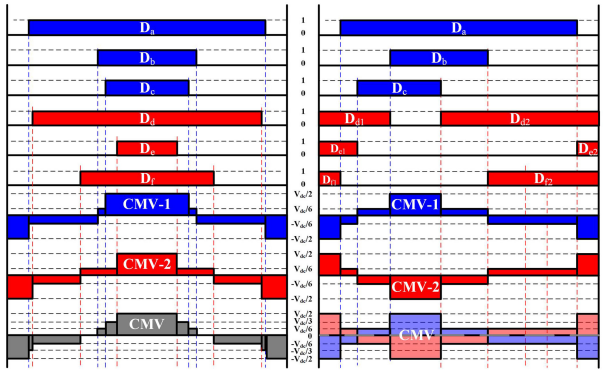

Fig. 3. Modulation scheme and the corresponding CMV for: CSPWM (left) and ZCMVM (right)

CMV modulation (ZCMVM) illustrated in the right plot of Fig. 3 [19]. Such a pulse shifting mechanism does not change the total number of switching actions in one switching period. Therefore, the switching loss remains the same as CSPWM or conventional SVM (CSVM).

A number of papers can be found investigating the CMV elimination for variable-speed drives. In [19], a CMV elimination modulation scheme is proposed for a dual three-phase permanent magnet synchronous motor. The proposed PWM shifting techniques realized an end-to-end cyclic PWM sequence to achieve CMV cancelation between two sets of three-phase windings. However, the algorithm is much more complex than the CSVM, and the proposed modulation method shows limited linearity range, where the high modulation and overmodulation scenarios are not considered. In [20], a CMV suppression strategy for synchronized SVM in the overmodulation region is proposed. However, due to three-phase structure limitation, the result can only restrict the peak CMV to fixed $V_{\mathrm{dc}}/6$ level without possibility for further reduction. Duran *et al.* [21] present an SVPWM algorithm for five-phase converters operating in the overmodulation region with forbidden zero vectors. Nevertheless, the zero vectors usage in the overmodulation range has already been gradually decreased. Avoiding zero vectors brings less effectiveness to the CMV reduction in this range. In addition, the odd phase number cannot effectively reduce the CMV. Multilevel inverters are proposed in [22] and [23] with the CMV reduction in overmodulation region. However, the cost of switches for three-level and five-level inverters is much higher than conventional six-phase structure, which is more preferred in the automotive application [24]. Instead of direct pulse shifting, a sawtooth carrier-based modulation is proposed in [25] for the asymmetrical DTM, which is intuitive but difficult to implement in digital controllers. Given different space vectors yield different CMV levels, some modulation methods are proposed in [26] and [27] to use specific space vector combinations for the CMV cancelation, where the limited vector usage constrains the vector plane, resulting in a limited linearity range. In [28], a new active zero state PWM (AZSPWM) for six-phase system is proposed where the CMV is reduced by one-third in the full linearity modulation range. Nevertheless, the side effects of AZSPWM, i.e., a much higher phase current ripple [29] is

yet to be solved. Besides, AZSPWM cannot eliminate CMV, making it unable to fully utilize the benefit of the DTMs. In [30] and [31], the differential-mode performance improvement for DTMs is investigated. The solutions focus more on the motor control algorithms instead of modulation mechanism, where the CM performance is not address.

In this article, a new modulation method to fully eliminate or reduce the CMV in for the full modulation span of a DTM drive system is proposed. The proposed method can fully eliminate the CMV when the modulation index is below 0.785, and significantly reduces the CMV in high or over modulation index. Different from previously proposed methods, this article is the few attempts to extends the CMV reduction method to the overmodulation range, and the proposed method is easy to implement. Section II builds the detailed mathematical model of the CMV for the proposed method. Section III uses the Simulink model to study the theoretical modulation behavior. In Section IV, the experimental result is presented to indicate its effectiveness in the full modulation range. Finally, Section V concludes this article.

II. Mathematical Model of CMV in DTM Systems

A. SPWM-Based ZCMVM for Modulation Index <0.785

Aligning the switch-ON/OFF edges to cancel the CMV is the precondition to cancel CMV in the DTM system. The question remains as whether this alignment can be applied in the whole switching period and extended to the whole modulation range. A mathematical model of CMV is important to explore such possibility. For SPWM, the duty cycle for each phase can be expressed as (3), where MI is the modulation index, x represents the phase number (a)–(f) and $\theta = 0, 2\pi/3, 4\pi/3, \pi/6, 5\pi/6, 3\pi/2$ for phases A—F, respectively. Here, two sets of windings, *ABC* and *DEF* have a 30° phase difference

$$D_x = \frac{1}{2} + \frac{2\mathrm{MI}}{\pi}\cos(\omega t + \theta) \tag{3}$$

$$\mathrm{MI} = \frac{\pi}{2} * \frac{V_{\mathrm{ref}}}{V_{\mathrm{dc}}}. \tag{4}$$

The PWM shifting and splitting rules can be referred to Fig. 3. Assume the PWM signal of phase A follows CSPWM without any shift or split, pulse shifting happens to phase B/C and pulse splitting happens to phase D/E/F. The newly split pulses at the beginning of each switching period denote as *d*1/*e*1/*f*1, and those at the end of the switching period denote as *d*2/*e*2/*f*2. As a result, (5)–(10) could be derived. If all of the switch-ON/OFF pairs can be aligned, D_{e2} must be equal to D_{f1}

$$D_{f1} = \frac{1 - D_a}{2} \tag{5}$$

$$D_{f2} = D_f - D_{f1} \tag{6}$$

$$D_{d1} = 1 - D_b - D_{f2} \tag{7}$$

$$D_{d2} = D_d - D_{d1} \tag{8}$$

$$D_{e1} = 1 - D_c - D_{d2} \tag{9}$$

$$D_{e2} = D_e - D_{e1}. \tag{10}$$

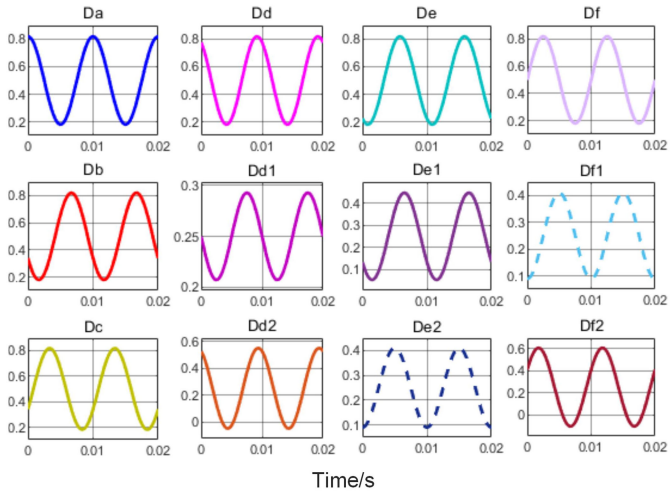

Fig. 4. ZCMVM modulation waveforms @MI = 0.5.

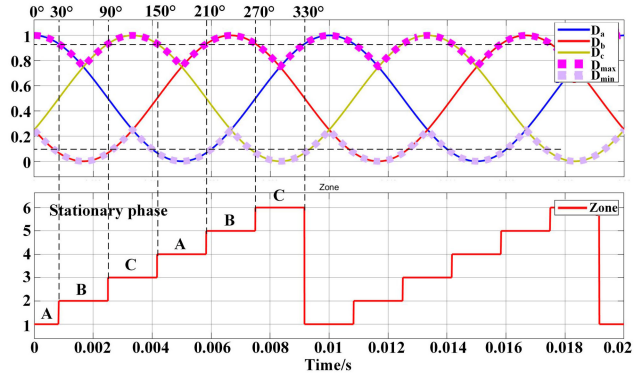

Fig. 5. ZCMVM zone division.

By substituting (3) into (4)–(10), D_{e2} and D_{f1} could be found as

$$D_{e2} = D_{f1} = \frac{1}{4} - \frac{MI}{\pi}\cos(\omega t). \tag{11}$$

This validates that shifting and splitting PWMs to align all switching pairs are theoretically feasible regardless of the modulation index MI. The challenge, however, is that such rules might not apply when the modulation index is high. For instance, when the modulation index is 0.5, Fig. 4 shows the original modulation waveforms for $D_{a\text{-}f}$ and the updated modulation waveforms for $D_{d\text{-}f1,2}$. The reference waveform of D_{f2} reaches below 0, which is physically not applicable thereby causing the phase current distortion.

The root cause is, in some cases, the PWM shifting and splitting rule twists the original duty cycle to force the edges to align. If phase A is always fixed as the reference phase, and the duty cycle of phase B/C becomes larger, the PWM shifting will be difficult to realize as there is left very limited room to move pulses of phase B/C. The solution is then to fix the phase with the too high or low of a duty cycle as the stationary phase while shifting the other two. To locate the stationary phase properly, Fig. 5 introduces the proposed zone division rule. By solving (12), a fundamental period could be divided into 6 zones by every 60°. The zone and corresponding stationary phase are given in

TABLE I
ZCMVM RULE

Zone 1,4	Stationary phase	S_a	S_b	S_c	S_d	S_e	S_f	ZCMV requirement
ωt(°)=0~30 & 150~210 & 330~360	A	0	0	0	1	1	1	D_{e2}=D_{f1}
		1	0	0	1	1	0	
		1	0	1	1	0	0	
		1	1	1	0	0	0	
		1	1	0	1	0	0	
		1	0	0	1	0	1	
		0	0	0	1	1	1	
Zone 2, 5	Stationary phase	S_a	S_b	S_c	S_d	S_e	S_f	ZCMV requirement
ωt(°)=30~90 & 210~270	B	0	0	0	1	1	1	D_{d1}=D_{f2}
		0	0	1	1	0	1	
		1	0	1	1	0	0	
		1	1	1	0	0	0	
		1	0	1	0	0	1	
		1	0	0	1	0	1	
		0	0	0	1	1	1	
Zone 3, 6	Stationary phase	S_a	S_b	S_c	S_d	S_e	S_f	ZCMV requirement
ωt(°)=90~150 & 270~330	C	0	0	0	1	1	1	D_{e1}=D_{d2}
		0	0	1	1	0	1	
		0	1	1	0	0	1	
		1	1	1	0	0	0	
		1	0	1	0	0	1	
		0	0	1	0	1	1	
		0	0	0	1	1	1	

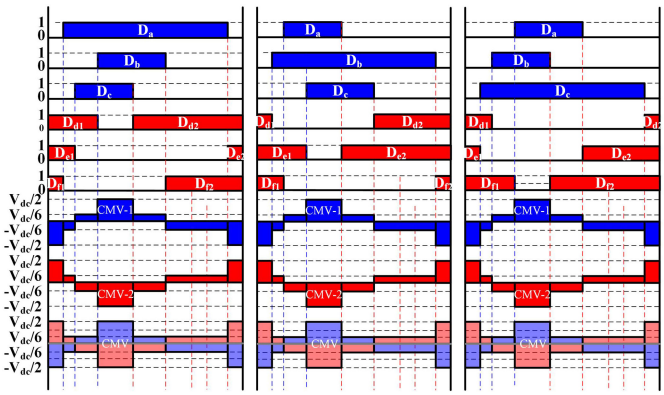

Fig. 6. ZCMVM pulse manipulation rules in different zones: (left) zone-1; 4 (middle) zone-2; 5 (right) zone-3; and 6.

Fig. 5 as well

$$D_{\max} = 1 - D_{\min}. \tag{12}$$

As the stationary phase varies from zone to zone, the ZCMV requirement also changes. The rule and corresponding switching sequency are given in Table I. Fig. 6 illustrates the PWM manipulation rule in each zone.

B. SVM-Based RCMVM for 0.785<Modulation Index<0.906

The proposed ZCMVM above is essentially an SPWM-based method, which limits the maximum linearity range to 0.785. To increase the dc bus voltage utilization, SVM is one of the most popular schemes where the third-order harmonic is injected. Whether the same ZCMV rule could apply to SVM then needs further investigation.

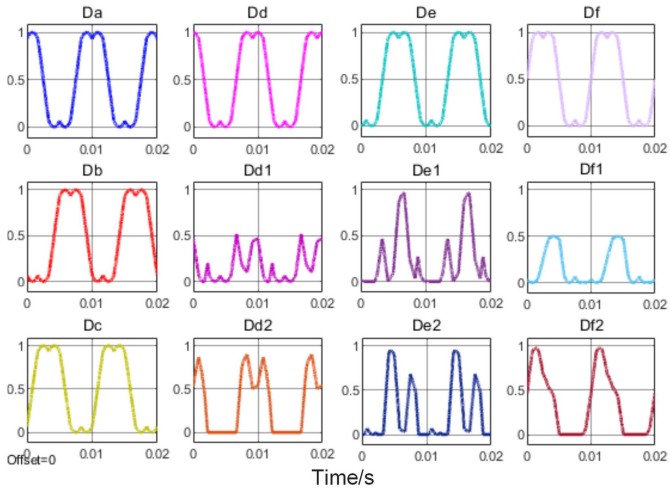

Fig. 7. RCMVM modulation waveforms @MI = 0.906.

For SVM, the duty cycle for each phase is formulated as (13), where x represents the phase index and $\theta = 0, 2\pi/3, 4\pi/3, \pi/6, 5\pi/6, 3\pi/2$ for phase A–F, respectively, and the $D_{3\mathrm{rd}}$ is the corresponding third-order harmonic injection. For each set of three-phase windings, the injected third voltage harmonics has a 30° difference

$$D_x = \frac{1}{2} + \frac{2MI}{\pi}\cos(\omega t + \theta) + D_{3\mathrm{rd}}. \tag{13}$$

If we follow Fig. 3 and (5)–(10), as shown in (14) D_{e2} is not equal D_{f1}. Therefore, the CMV cannot be eliminated. However, it still might reduce the CMV. If this is validated, the strategy for MI>0.785 can be renamed from ZCMVM to reduced-CMVM (RCMVM)

$$D_{e2} - D_{f1} = 3\left(D_{3\mathrm{rd}\_abc} + D_{3\mathrm{rd}\_def}\right). \tag{14}$$

Note the pulse manipulation needs to avoid phase current distortion. For example, in a split PWM, if the left piece cannot reach the edge alignment, the algorithm might force the alignment to happen by enlarging its length. As a result, the right piece length goes to negative, which is not feasible but only causes the phase current distortion. Fig. 7 shows the modulation waveforms for RCMVM when MI = 0.906. None of the adjusted duty cycles go below zero.

C. Overmodulation (0.906<Modulation Index<1)

For the conventional SVM, the overmodulation capability is necessary to maximize the dc bus voltage utilization. The work in [32] and [33] divided the overmodulation range into two segments, i.e., 0.906<MI<0.952 (mode I) and 0.952<MI<1 (mode II) and enhanced the total harmonic distortion (THD) performance compared with other overmodulation methods. This article based on their work adopts the same RCMVM method as the MI increases. The modulation waveforms for two overmodulation modes are shown in Fig. 8. Since in the overmodulation range the zero-vector operating time is reduced as well as the CMV, the total CMV reduction will not be as

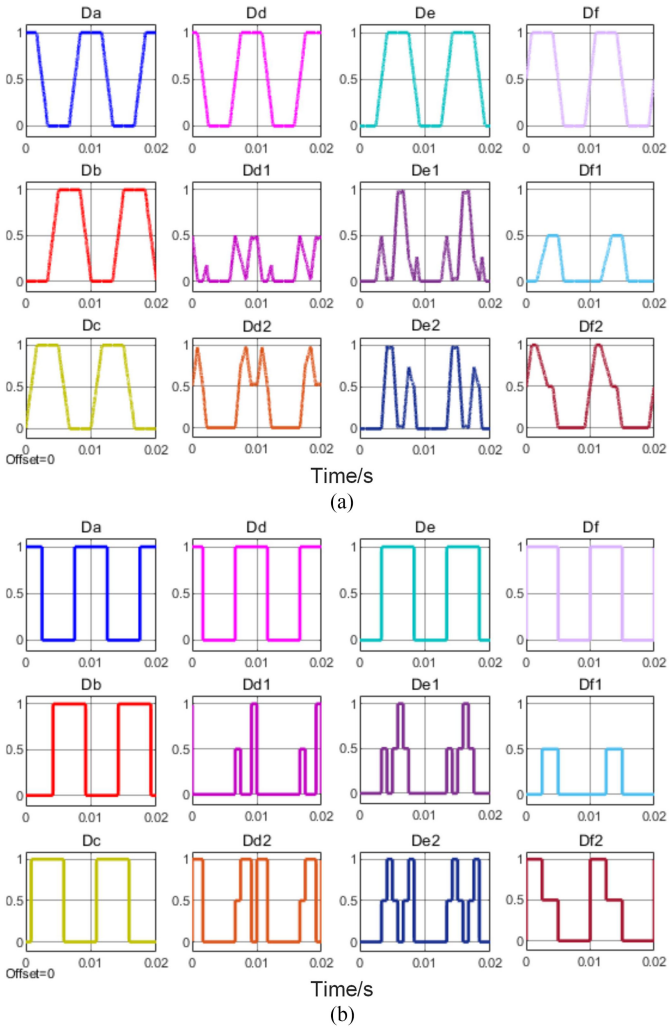

Fig. 8. RCMVM overmodulation waveforms. (a) MI = 0.95. (b) MI = 1.

significant as the linearity modulation range. When MI = 1, there are no differences between CSVM and the proposed RCMVM.

The mechanism of pulse manipulation in high modulation and overmodulation are the same, trying to align rising and falling edges to reduce the CMV. For the edges that fail to be aligned, the CMV will remain. This will happen not in the linearity modulation range, but in the high and over-modulation range. Fig. 9 illustrates the RCMVM operation, where the falling edge of D_c and rising edge of D_{d2} failed to be aligned.

As a result, the CMV between this interval still exist though the rest CMV in other areas is canceled.

Therefore, the proposed modulation scheme eliminates the CMV in low and medium modulation index range (0<M≤0.785) and reduces the CMV in high and overmodulation range (0.785 < M≤1). Therefore, this proposed modulation is named as zero/reduced CMVM (ZRCMVM).

III. Implementation and Simulation Results

Changing the carrier waveforms can realize the PWM shifting and splitting. However, for the proposed ZRCMVM, the PWM shifting/splitting occurs rapidly, causing significant difficulty in

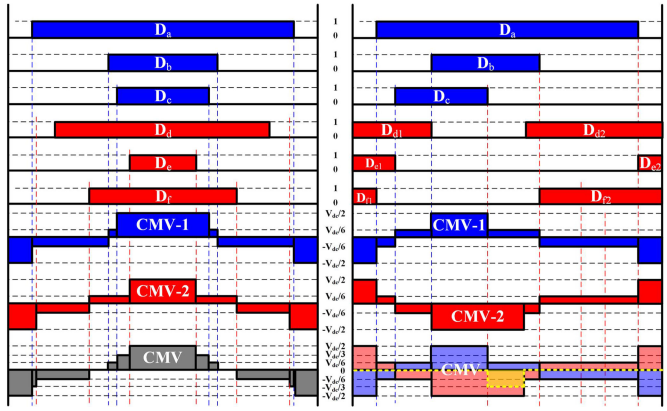

Fig. 9. Modulation scheme and the corresponding CMV for: CSVM (left) and RCMVM (right).

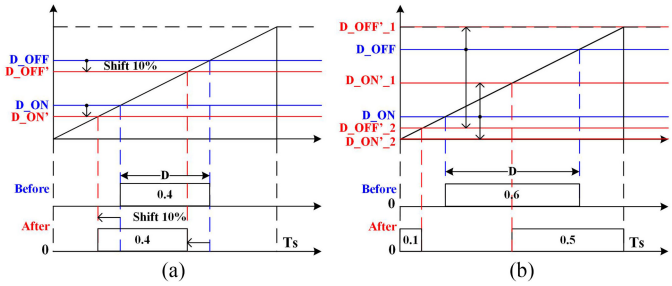

Fig. 10. Proposed pulse manipulation method. (a) Shifting. (b) Splitting.

carrier waveform modification. In this article, another efficient PWM manipulation method is proposed. As shown in Fig. 10, by calculating the ON/OFF duty cycle for each phase, we can compare it with the carrier and calculate the intermediate part with "AND" logic to obtain the duty cycle. By moving and splitting the ON/OFF duty-cycle, the PWM manipulation can be realized, as shown in (15)–(17). This method is applicable in an FPGA, utilizing Xilinx provided model-based coding tools for MATLAB/Simulink. In the EV domain, the high-resolution microcontrollers, such as FPGAs draw more attention nowadays. With the unique parallel computation capability, FPGAs can update duty cycles every switching period, reaching a higher control bandwidth. In this article, all control logics are realized through Xilinx System Generator. As the simulation is finished, the control code is ready as well to power two inverters for the DTM

$$D_{\text{on\_}x} = \frac{1}{2} - \frac{1}{2}\left(\frac{2\text{MI}}{\pi}\cos(\omega t + \theta) + \frac{1}{2}\right) \tag{15}$$

$$D_{\text{off\_}x} = \frac{1}{2} + \frac{1}{2}\left(\frac{2\text{MI}}{\pi}\cos(\omega t + \theta) + \frac{1}{2}\right) \tag{16}$$

$$D_x = D_{\text{off\_}x} - D_{\text{on\_}x}. \tag{17}$$

A. Low/Medium Modulation Range Simulation (0 < M≤0.785)

Fig. 11 simulates the CMV at different zones, where the modulation index is 0.3, dc bus voltage is set to 30 V for the

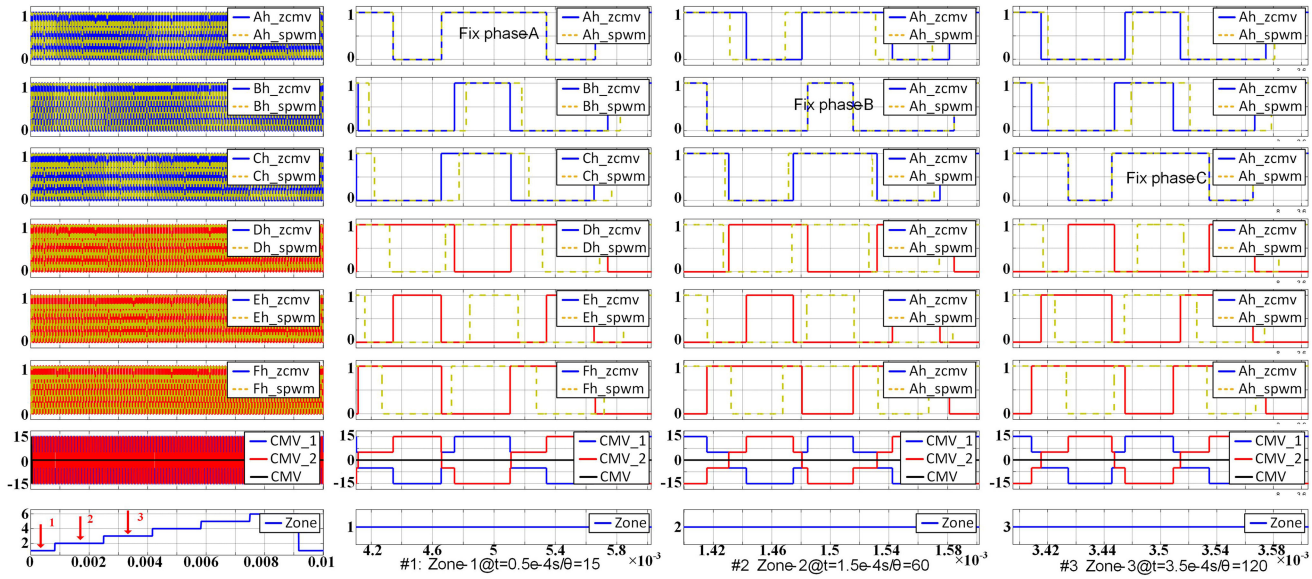

Fig. 11. Simulated CMV with ZRCMVM @MI = 0.3.

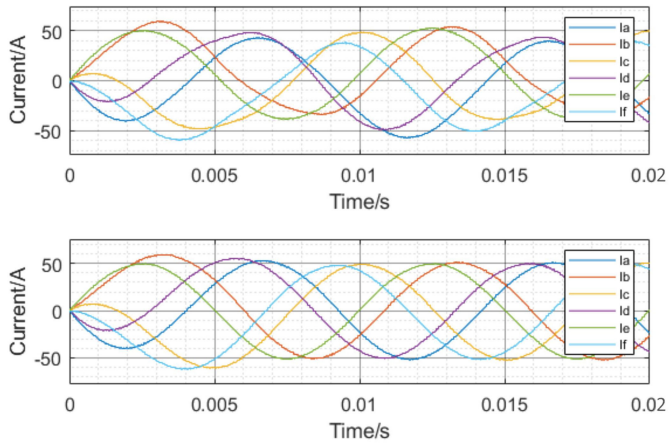

Fig. 12. Phase current waveform (simulation result). Top: without zone division; Bottom: with zone division.

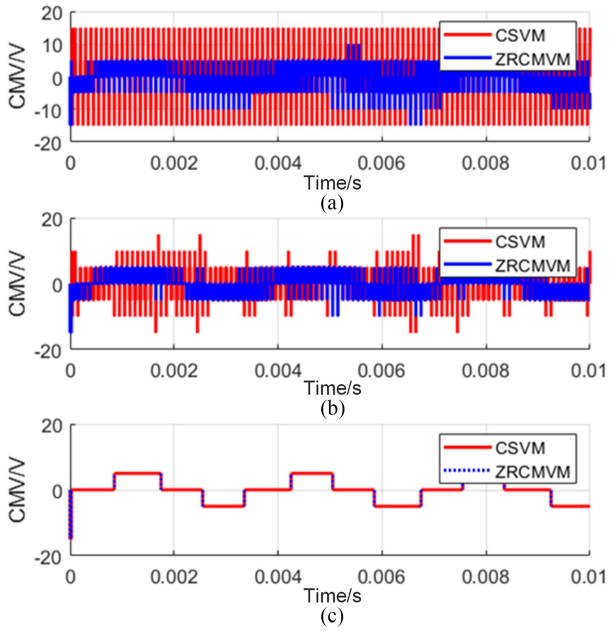

Fig. 13. CMV waveform under high/overmodulation. (a) MI = 0.906. (b) MI = 0.95. (c) MI = 1.

targeted 48 V motor drive application, switching frequency is 10 kHz and the fundamental frequency is 100 Hz. The CSPWM is also depicted as a green dashed line. Note that the dead time is not considered in this simulation. The PWMs for each phase are moved properly and the CMV is eliminated by ZRCMVM. In the CMV elimination process, the stationary phase changes every 60° to avoid potential phase current distortion. As a result, the load current is shown in Fig. 12. It shows with the proposed method of changing stationary phase per 60°, the phase current distortion disappears.

B. High/Overmodulation Range Simulation (0.785 < M≤1)

When the modulation index exceeds 0.785, the ZRCMVM is adjusted to the reduced-CMV mode. Fig. 13 shows the simulation result at the maximum linearity modulation point (MI = 0.906), the ending point of the overmodulation range mode 1 (MI = 0.95) and the full modulation point (MI = 1), respectively. In this range, the CMV starts to appear, although most of the $\pm V_{dc}/2$ components are eliminated due to the proper pulse manipulation. As the modulation enters the overmodulation range, the zero-vector time duration decreases, yielding a lower CMV even for the conventional SVM. When full modulation is achieved, there is no room for any PWM manipulation, and the performance of CMV reduction for CSVM and ZCMVM becomes identical. Such simulation results are aligned with the previous analytical analysis.

The fast Fourier transform (FFT) result of Fig. 13 is shown in Fig. 14. Aligned with the time domain analysis above, the proposed ZRCMVM although generates CMV still reduces CMV

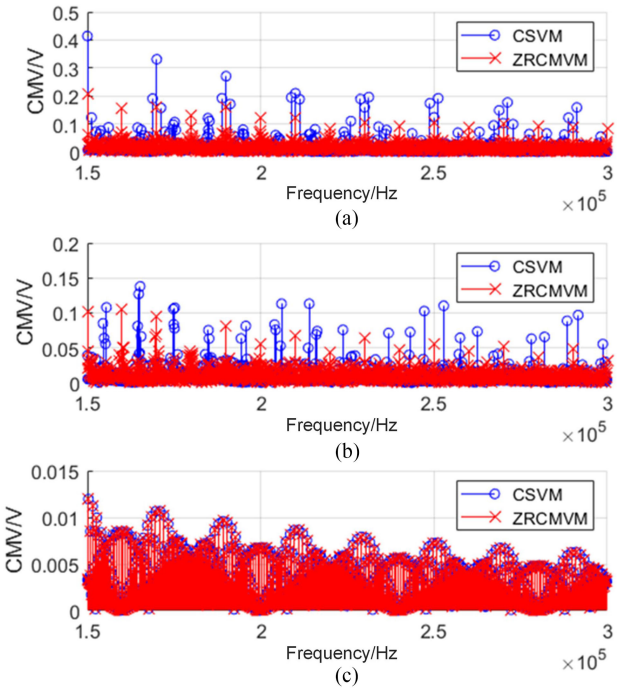

Fig. 14. CMV waveform under high/overmodulation (FFT results). (a) MI = 0.906. (b) MI = 0.95. (c) MI = 1.

compared with CSVM. Starting from the short-wavelength conductive CM EMI range (150–300 kHz) defined in CISPR-25, the maximum CMV components are reduced by half when MI = 0.906 and by one-third in the overmodulation mode I. When full modulation is realized, the CMV spectrum of CSVM and ZRCMVM becomes identical.

C. Differential-Mode Performance

The impact of various CMV reduction methods on the DM performance needs be closely monitored, given the phase current ripple and THD are closely related to PWM patterns. Some PWMs, such as AZSPWM, aim to reduce the CMV by splitting certain phase pulses to avoid using zero-vectors, but generate a much larger ripple current on both the dc-link side and the ac motor side. This not only worsens the harmonic performance but also causes acoustic noise during the operation. Therefore, the PWM manipulation process in the proposed ZRCMVM also needs to be evaluated. The simulation results of the input/output DM performance are shown in Figs. 15 and 16, performed with a 30 V dc bus voltage to fit the 48 V six-phase motor application, 10 kHz switching frequency and 100 Hz fundamental frequency. Here, CPWM denotes a combined PWM pattern, which uses CSPWM for MI<0.785 and CSVM for MI>0.785 to have a fair comparison with the proposed ZRCMVM.

At the input side, the dc-link capacitor current is critical to the dc-link capacitor selection, which strongly affects the system size. Fig. 15 shows the simulation result of the dc-link capacitor current for CPWM, ZRCMVM, and AZSPWM. The dc-link capacitor current of ZRCMVM, although slightly larger than CPWM, shows similarity to CPWM with a maximum difference of 5 A. Such small difference has very little impact on the

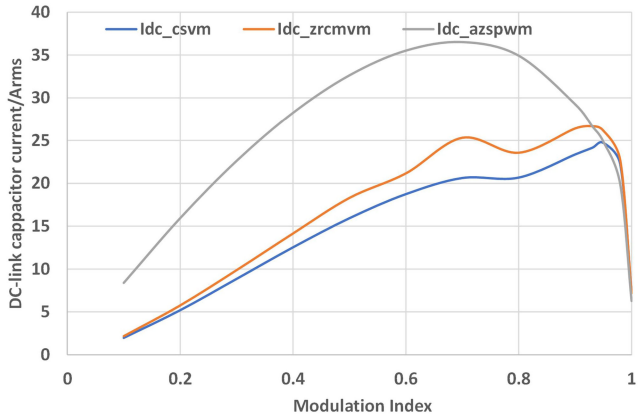

Fig. 15. DC-link capacitor current comparison.

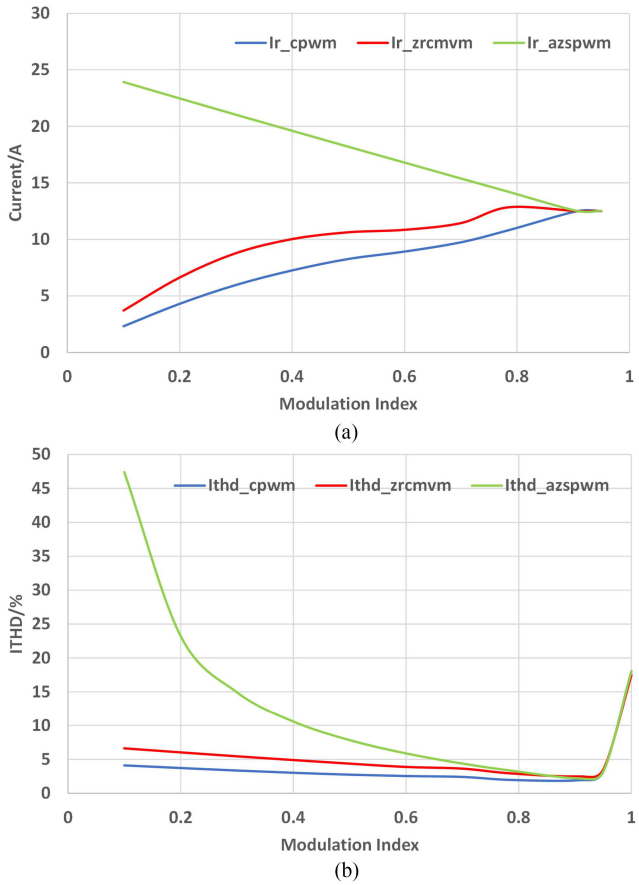

Fig. 16. Differential-mode impact at the output side. (a) Phase current ripple comparison. (b) Phase current THD comparison.

capacitor selection. For AZSPWM, the dc-link capacitor current ripple is significantly larger than ZRCMVM, which is in need of larger dc-link capacitors. Here, we simulated the current rms values.

At the output side, the major DM performance lies in the phase current ripple. Based on the simulation result shown in Fig. 16(a), the proposed ZRCMVM always has a higher ripple in the linearity modulation range than CPWM. As the modulation index increases, the ripple difference between ZRCMVM and CPWM decreases. In the overmodulation range, the difference

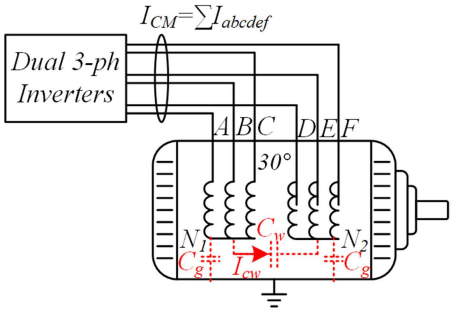

Fig. 17. Dual three-phase motor leakage current path.

is negligible. From the THD perspective as shown in Fig. 16(b), the current THD of ZRCMVM continuously drops as the modulation index increases. The overall gap is narrow and acceptable. Compared with ZCMVM and CPWM, AZSPWM has very poor performance in terms of both current ripple and THD, especially in the low modulation index range. Huang *et al.* [29] have proposed the phase current prediction model for AZSPWM to explain the essential cause, i.e., the split medium length PWM extends the time that the voltage imposed on the phase inductance, resulting in a larger current ripple. Such comparison shows the superiority of ZRCMVM when considering the DM performance that other reduced-CMV PWMs will not offer.

In addition to the grounding parasitic capacitor (C_g), there exists another leakage current path. As shown in Fig. 17, an inter-winding-sets parasitic capacitor (C_w) provides the path for leakage current to flow between two sets of three-phase windings, even though such leakage current does not contribute to the overall CM current.

Typically, the motor bearings are oil-lubricated, which has the insulation between the shaft and bearings [34]. However, in the motor starting process, the lubricant film has not well covered the bearings. The shaft voltage then will break down the film and generate leakage current (CM current) flowing to the ground through C_g. Compared with C_g, C_w is much smaller as the winding insulation is solid and evenly covered. The voltage across C_w is exactly the difference between the CMV for each three-phase winding sets (CMV1-CMV2). The causes leakage current which neither affects the system CM EMI performance nor ages the motor bearing.

In the simulation, the parasitic capacitance C_g and C_w is estimated as 530 and 110 pF, referred to [35]–[37]. The simulated waveforms at MI $= 0.5$ are attached in the Fig. 18.

Since the proposed ZRCMVM intends to force the CMV1 and CMV2 to be symmetrical along the horizontal axis, the voltage difference CMV1-CMV2 is then doubled, which is much larger than that under CSVM, as shown in top plot of Fig. 18. However, the inter-winding leakage current rms value is 0.4 mA under CSVM and only increased to 0.6 mA under ZRCMVM, not significantly enlarged as shown in the middle plot of Fig. 18. This is mainly due to small C_w. On the other hand, since the CMV is eliminated by ZRCMVM, the overall ground leakage current, i.e., CM current is also eliminated. As shown in the bottom plot of Fig. 18, the rms value of CM current under ZRCMVM is nearly 0 while that under CSVM is 2 mA. For MI>0.785, as

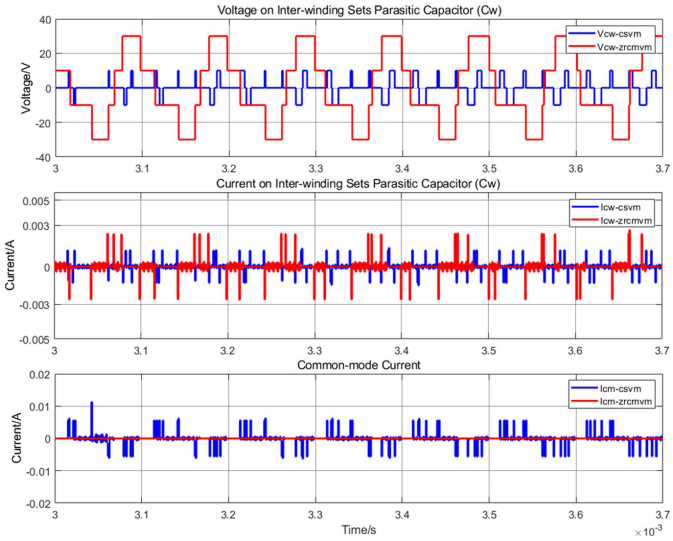

Fig. 18. Interwinding neutral voltage/current and CM current.

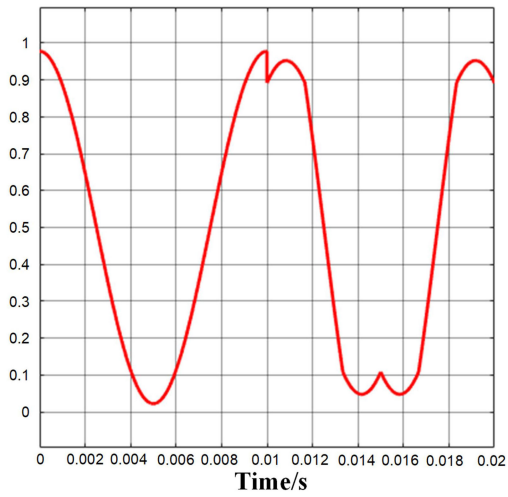

Fig. 19. Modulation waveform for an MI step change.

the symmetry of two CMV decreases, the voltage across C_w will also reduce, result in smaller interwinding leakage current. In conclusion, although the proposed modulation increases the leakage current between two winding sets, it is a component with less significance compared with the overall CM leakage current reduction.

D. Dynamic Performance

Through the whole modulation span, there are two different modulation mechanisms. For MI≤0.785, the strategy is CSPWM-based ZCMV modulation. And for MI>0.785, the strategy is CSVM-based RCMV modulation. In the motor drive applications, the modulation index varies dynamically as the motor changes the status. Therefore, the transient performance when the modulation index passes through the boundary should be investigated.

Given the step change of the MI from 0.75–0.82 at 0.01s. As shown in Fig. 19, the sinusoidal modulation waveform will

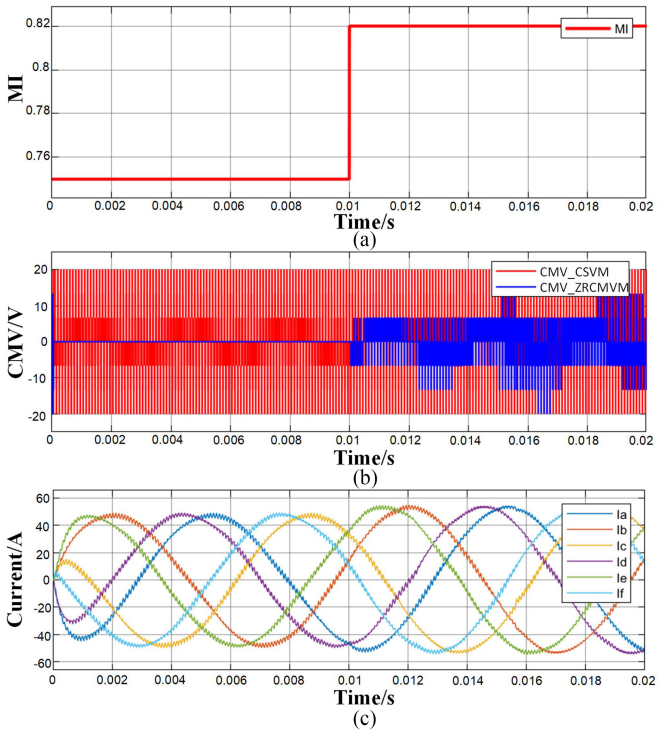

Fig. 20. Transient process for region switch. (a) Modulation index. (b) CMV. (c) Three-phase current.

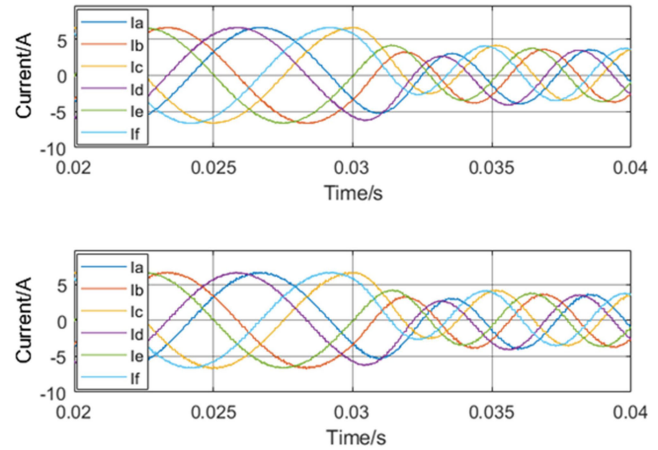

Fig. 21. Transient process for speed change. Top: CSPWM; Bottom: ZR-CMVM.

change to the SVM waveform, which is injected with third-order harmonics.

The simulation of the transient process for a region switch is shown in Fig. 20. As the MI jumps into RCMV modulation range, the CMV starts to appear. The amplitude of the phase current increases accordingly with no inrush. This is another support for the conclusion in Section III-C that the proposed modulation method shows less impact on the differential-mode performance.

The motor speed change refers to a fundamental frequency variation. Fig. 21 shows the six-phase current waveform and CMV waveform during a fundamental frequency change from 100 to 200 Hz at 0.03 s. The transition during the speed change is

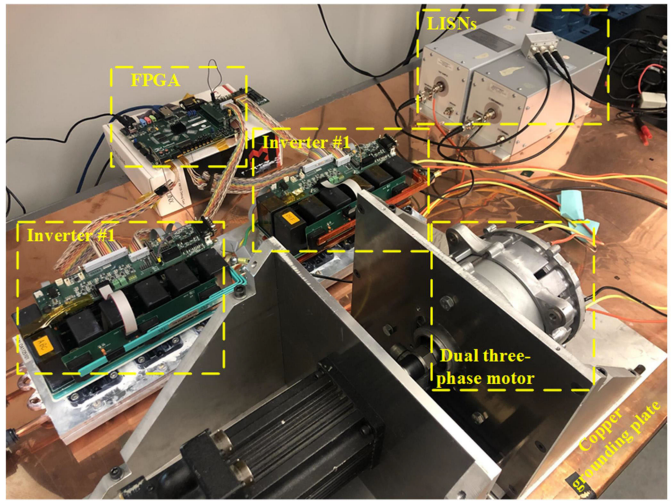

Fig. 22. Test bench.

TABLE II
TEST BENCH PARAMETERS

Item	Value	Unit
DC bus voltage	30	V
Output Power	5	kW
Switching frequency (fs)	10	kHz
Fundamental frequency (f0)	100	Hz

smooth with no spikes or fluctuations, and the CMV elimination performance is not affected.

The transient simulation shows that the system dynamic performance is the same with CSPWM/CSVM, this is because the proposed ZRCMVM does not change the modulation waveform, but directly redistributes the PWM pulse generated by CSPWM/CSVM. Therefore, from the space vector point of view, the trajectory never changes. This applies to the whole modulation range. The only difference it brings to the system on DM is the current ripple change due to the irregular pulse assignment.

IV. EXPERIMENTAL VALIDATION

With the Xilinx System Generator toolbox, the Simulink model can be translated into the FPGA code. To set up the experimental validation, two three-phase inverters are designed to set up a DTM drive test bench, as shown in Fig. 22. The motor is rated at 48 V/10 kW with two separated neutral points. The 48 V technology has been widely accepted in mild hybrid EVs, which enable considerable savings in fuel consumption with moderate additional costs [38]–[41]. Therefore, in this article, we used such a 48 V DTM as an example.

The detailed test bench parameters are given in Table II. The whole system sits on a grounded copper plate on the basis of EMI measurement criteria.

A. CMV Measurement

The CMV waveform is measured in four different modulation zones, as shown in Fig. 23; the CMV measurement is

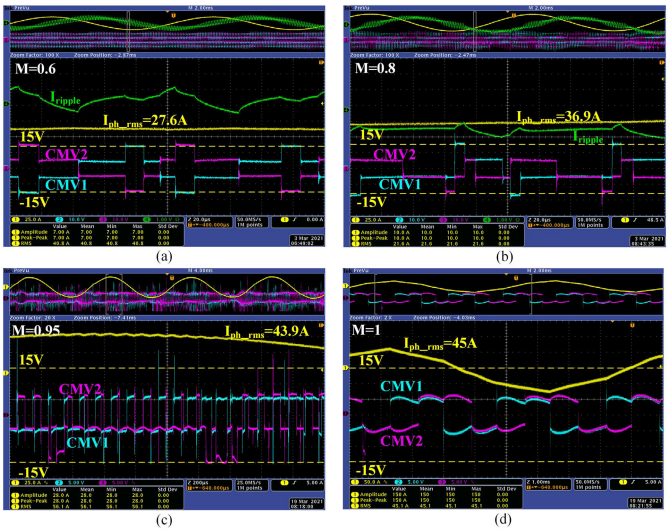

Fig. 23. CMV Waveform. (a) ZCMV in linearity range (MI = 0.6). (b) RCMV in linearity range (MI = 0.8). (c) RCMV in overmodulation range mode-I (MI = 0.6). (d) RCMV in overmodulation range mode-II (MI = 1, full modulation).

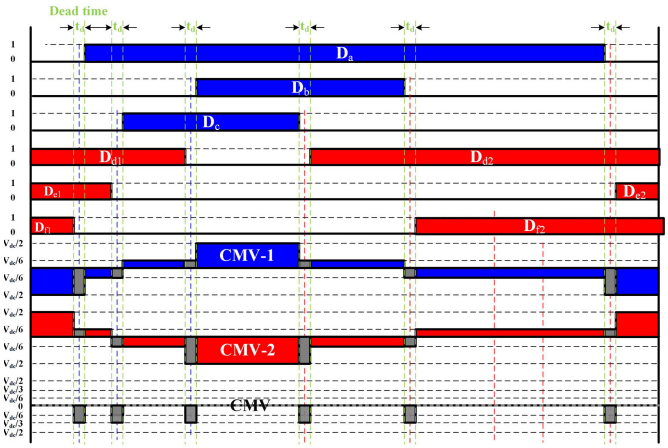

Fig. 24. Dead time effect on CMV.

processed in the ZCMV-linearity range (MI = 0.6), RCMV-linearity range (MI = 0.8), RCMV-overmodulation mode I (MI = 0.95), and RCMV-Full modulation (MI = 1). Here, CMV1 and CMV2 represent the CMV on each set of three-phase windings, respectively.

According to the proposed CMV reduction strategy, for MI<0.785, the waveform of CMV1 and CMV2 is mirror-symmetrical along the time axis to cancel each other thereby eliminating the overall CMV. For MI>0.785 the CMV is reduced, even the waveform of CMV1 and CMV2 is not vertically mirrored. The experimental result shows good execution of the ZRCMVM method, despite the CMV spikes caused by the 300 ns dead time. Specifically, the unexpected CMV spike happens at the instants when two phases commutate simultaneously [42]. The dead time effect on is shown in Fig. 24. Due to the existing of dead time, some CMV patterns are extended for a short period, which makes the symmetrical CMV on each three-phase set become asymmetry on the edge. As a result, at each commutation point, a $V_{dc}/3$ CMV pulse will be generated.

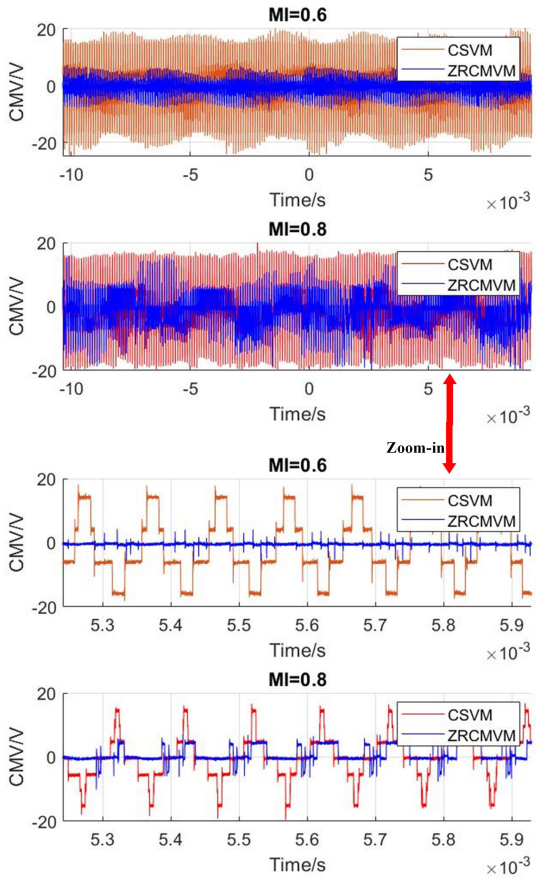

Fig. 25. CMV comparison between CSVM and ZRCMVM in the linearity range.

For conventional center-aligned modulation, the simultaneous phase commutation cased CMV spike is negligible since the commutation always happens at the edge of zero vector. In addition, the two-phase simultaneous commute only happens once in a sector plain (twice for six-phase as there exist a 30° vector plain rotation). As a result, the CMV cause by dead time is minimal. However, for the proposed ZRCMVM, each switching edge pair is intentionally assigned to be aligned, which means the two-phase simultaneous commutation happens in every switching cycle. Therefore, the dead time caused CMV spikes have more impact on the CM EMI performance for the ZRCMVM. There are many literatures has discussed about the dead time effect on the CMV and the corresponding compensation work. However, current direction and of output voltage polarity detection are typically needed, which requires extra hardware support, such as current or voltage sensor [43]–[46]. Since this article targets on the new modulation method mechanism, the dead time compensation will be included in the future work instead of further investigation here.

At the same test condition, the measurement data of CSVM is also collected and compared with the proposed ZRCMVM, as shown in Fig. 25–27. In the linearity range, compared with CSVM, ZRCMVM eliminates the CMV voltage levels in medium and low modulation index and reduces CMV in the high modulation index range. In this stage, the superiority of

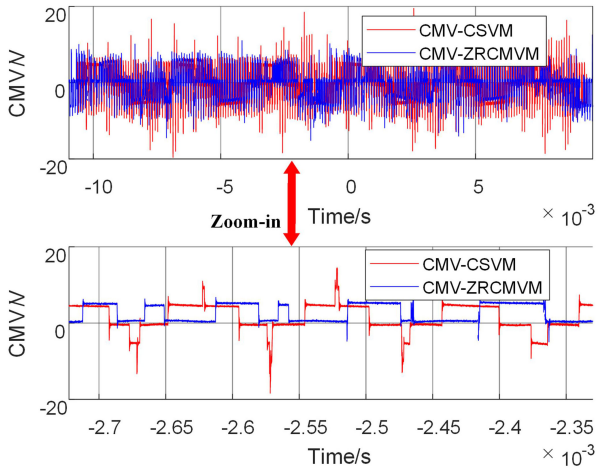

Fig. 26. CMV comparison between CSVM and ZRCMVM in overmodulation range.

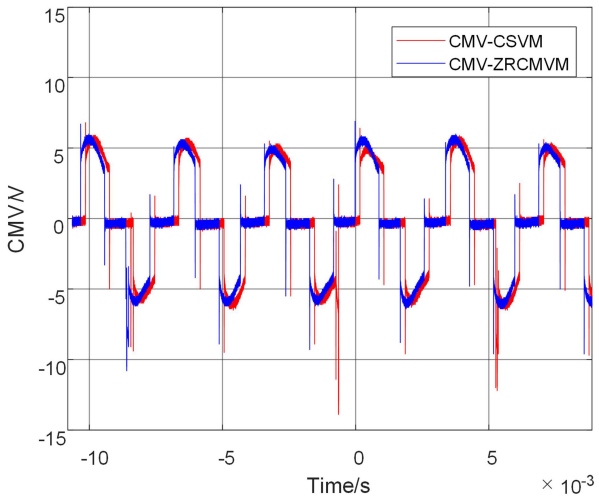

Fig. 27. CMV comparison between CSVM and ZRCMVM at full modulation.

ZRCMVM is significant as it enters the overmodulation range, the CSVM also reduces the zero-state vector operation time with less zero-state duration. As a result, the CMV of CSVM starts to decrease. Though ZRCMVM still shows better CMV reduction performance, the gap between CSVM and ZRCMVM is narrowed. Eventually, when the system reaches the full modulation, the two modulation schemes have no difference on the CMV performance, as shown in Fig. 27, and the two CMV waveforms both become three-level ($-V_{\rm dc}/6$, 0, $V_{\rm dc}/6$). Such CMV behavior is aligned with the theoretical analysis in Section II and simulation result in Section III.

The experimental results above provide a direct performance comparison between CSVM and ZRCMVM through the time domain CMV waveform. However, in the motor drive system, the essential harm that the inverter brings to the motor lifespan is caused by the CMC. To further confirm the effectiveness of the proposed ZRCMVM, a quantitative comparison of the CMC is necessary, which relies on the line impedance stabilization network (LISN). LISN provides a stable and normalized source impedance (50 Ω in this test) for the CMC measurement and

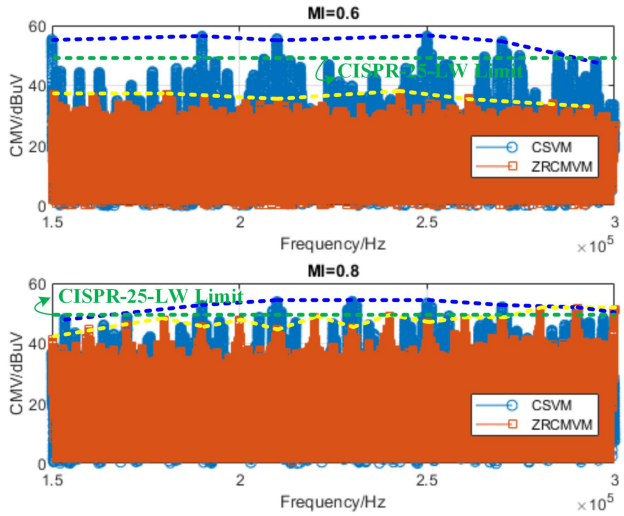

Fig. 28. CMC spectrum comparison in the linearity modulation range.

prevents the external noise from interfering with the source side [47]. The measured CMC is then sent to the EMI analyzer through the power combiner, which allows the CMC component to pass while suppressing the DM component. The whole system sits on a copper grounding plate, where the inverter heatsink, motor case, and LISN are grounded.

The proposed model aims to eliminate the CMV profile through modulation, however, some *dv/dt* components still exist because of the switching actions and dead time effect. Therefore, the high-frequency EMI noise dominated by the high-speed transient processes will not be effectively reduced compared to CSVM. Considering the CM filter is typically designed with respect to the low-frequency range as the high-frequency components are relatively easier to damp, the CM EMI spectrum on the low-frequency conductive range is measured, as shown in Figs. 28–30. This range (150–300 kHz) is defined in CISPR-25 as the longwave broadcast band, which is strongly affected by the modulation-based CMV reduction.

In the linearity range when MI = 0.6, the CMC reduction is significant. The maximum reduction is around 23 dBμV. Note, such measured voltage is the CMC multiplied with 50 Ω-resistance inside the LISN. A drastic reduction of the CMC at low-frequency range is attributed to the proposed ZRCMVM. For MI = 0.8, the modulation aims at RCMV, and the maximum reduction is lowered to around 8 dBμV, still exhibiting ∼60% CMC reduction.

In the overmodulation range, as the system approaching full modulation, the theoretical CM performance of both modulation schemes should gradually merge. The CM EMI spectrum of CSVM and ZRCMVM are approaching each other due to the reduced CMV of CSVM itself. At the end of overmodulation mode I (MI = 0.95), the maximum reduction on the spectrum envelop is ∼6 dBμV. From the obtained spectrum at MI = 1, the envelopes for CSVM and ZRCMVM are nearly overlapped. Therefore, the EMI spectrum measurements confirm the ZRCMVM performance behavior through a full modulation span, which are modeled in the previous sections.

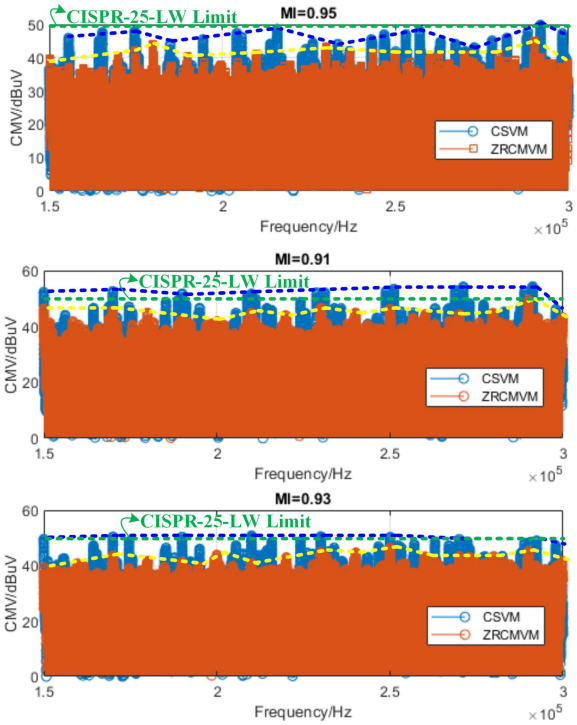

Fig. 29. CMC spectrum comparison in the overmodulation range (mode I).

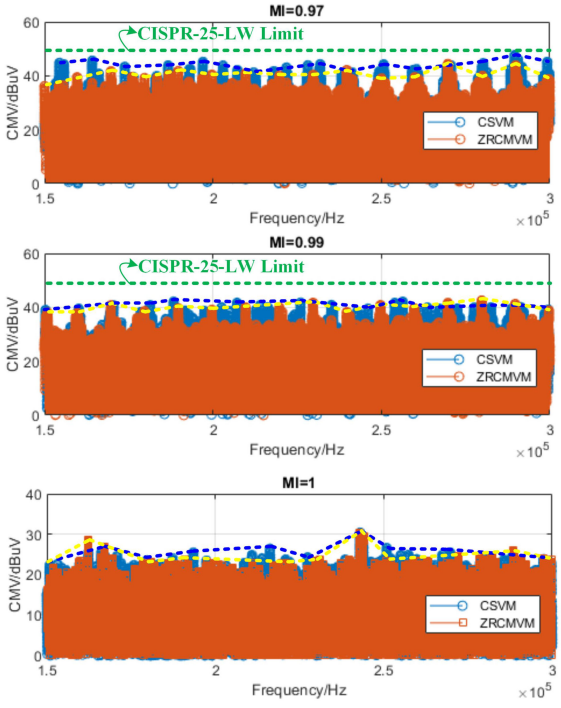

Fig. 30. CMC spectrum comparison in the overmodulation range (mode II).

B. DM Performance Measurement

The measured phase current in different modulation range is shown in Fig. 31 with an inductive load. The phase current quality in the linearity range is secured by ZRCMVM, however, in the overmodulation range the current starts to distort. In Section III, the differential impact of ZRCMVM is investigated. It shows

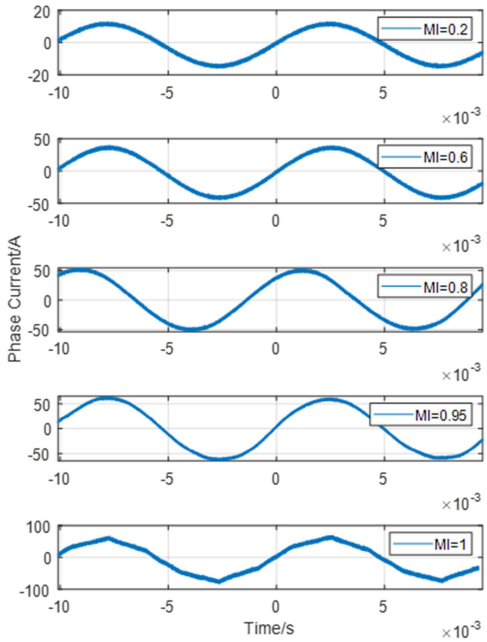

Fig. 31. Phase current waveforms.

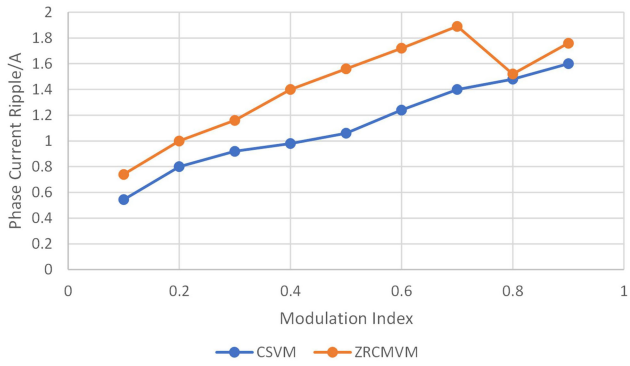

Fig. 32. Phase current ripple measurement.

that even though ZRCMVM is based on pulse manipulation, the phase current ripple caused by ZRCMVM is not significantly larger than CSVM.

To further verify the differential-mode performance, the tested phase current ripple is captured through an RF current probe. As shown in Fig. 32, the modulation index varies from 0.1 to 0.9, where the corresponding phase current $t_{\rm rms}$ value increases from 4.75 to 39 A. The phase current ripple of ZRCMVM is not obviously larger than CSVM. The total ripple to phase current rms ratio increment is less than 1.7%. Such performance not only prevents worsening phase current THD but also avoids loud acoustic noise, especially when the switching frequency is below 20 kHz.

V. Conclusion

This article proposed a CMV elimination/reduction modulation scheme that covers the full modulation range. In the low/medium modulation range ($0 < M \leq 0.785$), the modulation is CSPWM based, where the objective is to fully eliminate the

CMV. In the high/overmodulation range ($0.785 < M \leq 1$) when SVPWM is adopted, due to the need for third-order harmonic injection, zero CMV is hard to realize. The proposed modulation strategy, however, can still reduce the CMV. The overall CMV is drastically reduced from the perspective of full modulation operation. In summary, the proposed ZRCMVM has following advantages.

1) The modulation is based on the basic PWM methods, only adding an additional pulse manipulation process. The overall implementation difficulty is low.
2) Nearly 80% of operation points can work under zero CMV conditions, which covers most realistic scenarios. The rest of the operation points can still see significant CMV reduction.
3) Compared with some reduced-CMV modulation methods, e.g., AZSPWM, the phase current ripple caused by the pulse manipulation in ZRCMVM is much smaller, especially in the high/overmodulation range. Though the third-order harmonic injection is applied when MI $>$ 0.785, due to the high modulation index, the ripple has negligible difference compared to CSVM. This will benefit the current quality and lower acoustic noise.
4) The total switching loss of ZRCMVM is the same with CSVM as no extra switching action is introduced. Compared to some methods adding extra switching actions to reduce CMV, the efficiency using proposed ZRCMVM will not be reduced.

With the Xilinx system generator platform, the simulated modulation algorithm is easily converted to the FPGA code. The experimental results prove the effectiveness of ZRCMVM on the CMV reduction, without sacrificing the DM performance in the full modulation range. It is worth pointing out that the pulse shifting/splitting method is not restricted to any specific modulation scheme. For various third order harmonic injections (triangle wave is injected in this article for CSVM), the same approach might also apply. The future work is: to extend this method to other modulations, for example, DPWM; and to build its analytically model of the phase-current ripple and dc-link ripple, which will further guide the component selection in the 48 V EV drive system.

REFERENCES

[1] E. Levi *et al.*, "Multiphase induction motor drives-a technology status review," *IET Electr. Power Appl.*, vol. 1, no. 4, pp. 489–516, 2007.

[2] E. Levi, "Multiphase electric machines for variable-speed applications," *IEEE Trans. Ind. Electron.*, vol. 55, no. 5, pp. 1893–1909, May 2008.

[3] Q. Yan, X. Yuan, Y. Geng, A. Charalambous, and X. Wu, "Performance evaluation of split output converters with SiC MOSFETs and SiC Schottky diodes," *IEEE Trans. Power Electron.*, vol. 32, no. 1, pp. 406–422, Jan. 2017.

[4] R. Bojoi *et al.*, "Industrial power conversion systems department-industrial drives committee-digital field-oriented control for dual three-phase induction motor drives," *IEEE Trans. Ind. Appl.*, vol. 39, no. 3, pp. 752–760, May/Jun. 2003.

[5] G. K. Singh, K. Nam, and S. K. Lim, "A simple indirect field-oriented control scheme for multiphase induction machine," *IEEE Trans. Ind. Electron.*, vol. 52, no. 4, pp. 1177–1184, Aug. 2005.

[6] S. Hu, Z. Liang, W. Zhang, and X. He, "Research on the integration of hybrid energy storage system and dual three-phase PMSM drive in eV," *IEEE Trans. Ind. Electron.*, vol. 65, no. 8, pp. 6602–6611, Aug. 2018.

[7] S. Bhattacharya, D. Mascarella, G. Joos, J.-M. Cyr, and J. Xu, "A dual three-level T-NPC inverter for high-power traction applications," *IEEE J. Emerg. Sel. Topics Power Electron.*, vol. 4, no. 2, pp. 668–678, Jun. 2016.

[8] X. Jiang, W. Huang, R. Cao, Z. Hao, and W. Jiang, "Electric drive system of dual-winding fault-tolerant permanent-magnet motor for aerospace applications," *IEEE Trans. Ind. Electron.*, vol. 62, no. 12, pp. 7322–7330, Dec. 2015.

[9] Y. Zhao and T. A. Lipo, "Space vector PWM control of dual three-phase induction machine using vector space decomposition," *IEEE Trans. Ind. Appl.*, vol. 31, no. 5, pp. 1100–1109, Sep./Oct. 1995.

[10] K. A. Chinmaya and G. K. Singh, "Experimental analysis of various space vector pulse width modulation (SVPWM) techniques for dual three-phase induction motor drive," *Int. Trans. Elect. Energy Syst.*, vol. 29, no. 1, 2019, Art. no. 2678.

[11] Ó. López *et al.*, "Space-vector PWM with common-mode voltage elimination for multiphase drives," *IEEE Trans. Power Electron.*, vol. 31, no. 12, pp. 8151–8161, Dec. 2016.

[12] A. L. Julian, "Active common mode voltage reduction in voltage source inverters," Ph.D. dissertation, Dept. Elect. Comput. Eng., Univ. Wisconsin–Madison, Madison, WI, USA, 1997.

[13] D. Jiang, F. Wang, and J. Xue, "PWM impact on CM noise and AC CM choke for variable-speed motor drives," *IEEE Trans. Ind. Appl.*, vol. 49, no. 2, pp. 963–972, Mar./Apr. 2013.

[14] S. Ogasawara and H. Akagi, "Modeling and damping of high-frequency leakage currents in PWM inverter-fed AC motor drive systems," *IEEE Trans. Ind. Appl.*, vol. 32, no. 5, pp. 1105–1114, Sep./Oct. 1996.

[15] D. Busse, J. Erdman, R. J. Kerkman, D. Schlegel, and G. Skibinski, "Bearing currents and their relationship to PWM drives," *IEEE Trans. Power Electron.*, vol. 12, no. 2, pp. 243–252, Mar. 1997.

[16] H. Akagi and T. Shimizu, "Attenuation of conducted EMI emissions from an inverter-driven motor," *IEEE Trans. Power Electron.*, vol. 23, no. 1, pp. 282–290, Jan. 2008.

[17] J. M. Erdman, R. J. Kerkman, D. W. Schlegel, and G. L. Skibinski, "Effect of PWM inverters on AC motor bearing currents and shaft voltages," *IEEE Trans. Ind. Appl.*, vol. 32, no. 2, pp. 250–259, Mar./Apr. 1996.

[18] L. Wang, Y. Shi, and H. Li, "Anti-EMI noise digital filter design for a 60-kW five-level SiC inverter without fiber isolation," *IEEE Trans. Power Electron.*, vol. 33, no. 1, pp. 13–17, Jan. 2018.

[19] Z. Shen, D. Jiang, Z. Liu, D. Ye, and J. Li, "Common-mode voltage elimination for dual two-level inverter-fed asymmetrical six-phase PMSM," *IEEE Trans. Power Electron.*, vol. 35, no. 4, pp. 3828–3840, Aug. 2019.

[20] Y. Duan *et al.*, "Synchronized SVPWM strategy for common mode voltage reduction of high power inverters in the overmodulation region," in *Proc. 22nd Int. Conf. Elect. Mach. Syst.*, 2019, pp. 1–5.

[21] M. J. Duran, J. Prieto, and F. Barrero, "Space vector PWM with reduced common-mode voltage for five-phase induction motor drives operating in overmodulation zone," *IEEE Trans. power Electron.*, vol. 28, no. 8, pp. 4030–4040, Aug. 2013.

[22] P. N. Tekwani, R. S. Kanchan, and K. Gopakumar, "A dual five-level inverter-fed induction motor drive with common-mode voltage elimination and DC-link capacitor voltage balancing using only the switching-state redundancy—Part I," *IEEE Trans. Ind. Electron.*, vol. 54, no. 5, pp. 2600–2608, Oct. 2007.

[23] P. P. Rajeevan and K. Gopakumar, "A hybrid five-level inverter with common-mode voltage elimination having single voltage source for IM drive applications," *IEEE Trans. Ind. Appl.*, vol. 48, no. 6, pp. 2037–2047, Nov./Dec. 2012.

[24] S. Sharma, M. V. Aware, and A. Bhowate, "Symmetrical six-phase induction motor-based integrated driveline of electric vehicle with predictive control," *IEEE Trans. Transp. Electrific.*, vol. 6, no. 2, pp. 635–646, Jun. 2020.

[25] Z. Liu, Z. Zheng, Z. Peng, Y. Li, and L. Hao, "A Sawtooth carrier-based PWM for asymmetrical six-phase inverters with improved common-mode voltage performance," *IEEE Trans. Power Electron.*, vol. 33, no. 11, pp. 9444–9458, Nov. 2018.

[26] L. Fangke, L. Haifeng, L. Yongdong, and C. Jianyun, "A modulation method to eliminate common-mode voltage of dual three-phase motor," in *Proc. IEEE Transp. Electrific. Conf. Expo.*, 2019, pp. 1–5.

[27] S. A. Yerkal, M. V. Aware, B. S. Umre, M. Waghmare, and A. Kumar, "Common mode voltage elimination in a three-to-six phase indirect matrix converter using SVM technique," in *Proc. IEEE Int. Conf. Power Electron., Drives Energy Syst.*, 2020, pp. 1–6, doi: 10.1109/PEDES49360.2020.9379372.

[28] J.-H. Baik, S.-W. Yun, and J.-Y. Yoo, "A new active zero state PWM for six-phase inverter," in *Proc. 10th Int. Conf. Power Electron. ECCE Asia*, 2019, pp. 933–938.
[29] Y. Huang *et al.*, "Analytical characterization of CM and DM performance of three-phase voltage-source inverters under various PWM patterns," *IEEE Trans. Power Electron.*, vol. 36, no. 4, pp. 4091–4104, Apr. 2021.
[30] Z. Wang, X. Wang, X. Yang, C. Wen, Y. Gong, and Y. Hu, "Mitigation of DC-link current ripple for dual three-phase flux-adjustable hybrid PMAC drives using collaborative switching strategy," *IEEE Trans. Ind. Electron.*, vol. 67, no. 9, pp. 7202–7216, Sep. 2010.
[31] Y. Ren and Z.-Q. Zhu, "Reduction of both harmonic current and torque ripple for dual three-phase permanent-magnet synchronous machine using modified switching-table-based direct torque control," *IEEE Trans. Ind. Electron.*, vol. 62, no. 11, pp. 6671–6683, Nov. 2015.
[32] D.-C. Lee and G.-M. Lee, "A novel overmodulation technique for space-vector PWM inverters," *IEEE Trans. Power Electron.*, vol. 13, no. 6, pp. 1144–1151, Nov. 1998.
[33] J. Holtz, W. Lotzkat, and A. M. Khambadkone, "On continuous control of PWM inverters in the overmodulation range including the six-step mode," *IEEE Trans. power Electron.*, vol. 8, no. 4, pp. 546–553, Oct. 1993.
[34] J. D. Neely, "Fault types and reliability estimates in permanent magnet AC motors," M.S. thesis, Dept. Elect. Comput. Eng., Michigan State Univ., East Lansing, MI, USA, 2005.
[35] J. Luszcz and K. Iwan, "AC motor transients and EMI emission analysis in the ASD by parasitic resonance effects identification," in *Proc. Eur. Conf. Power Electron. Appl.*, 2007, pp. 1–9.
[36] J. Luszcz and K. Iwan, "Modelling conducted EMI in inverter-fed AC motor," in *Proc. IEEE Compat. Power Electron.*, 2005, pp. 209–212.
[37] J.-K. Park, T. R. Wellawatta, S.-J. Choi, and J. Hur, "Mitigation method of the shaft voltage according to parasitic capacitance of the PMSM," *IEEE Trans. Ind. Appl.*, vol. 53, no. 5, pp. 4441–4449, Sep./Oct. 2017.
[38] R. Bojoi, A. Cavagnino, M. Cossale, and A. Tenconi, "Multiphase starter generator for a 48-V mini-hybrid powertrain: Design and testing," *IEEE Trans. Ind. Appl.*, vol. 52, no. 2, pp. 1750–1758, Apr. 2016.
[39] J. Seong *et al.*, "DBC-Packaged inverter power module for integrated motor-inverter design used in 48 v mild hybrid starter-generator (MHSG) system," *IEEE Trans. Veh. Technol.*, vol. 68, no. 12, pp. 11704–11713, Dec. 2019.
[40] A. Cavagnino, A. Tenconi, and S. Vaschetto, "Experimental characterization of a belt-driven multiphase induction machine for 48-V automotive applications: Losses and temperatures assessments," *IEEE Trans. Ind. Appl.*, vol. 52, no. 2, pp. 1321–1330, Apr. 2016.
[41] J. Seong *et al.*, "Multiphysics simulation analysis and design of integrated inverter power module for electric compressor used in 48-V mild hybrid vehicles," *IEEE J. Emerg. Sel. Topics Power Electron.*, vol. 7, no. 3, pp. 1668–1676, Sep. 2019.
[42] Y.-S. Lai and F.-S. Shyu, "Optimal common-mode voltage reduction PWM technique for inverter control with consideration of the dead-time effects–Part I: Basic development," *IEEE Trans. Ind. Appl.*, vol. 40, no. 6, pp. 1605–1612, Nov./Dec. 2004.
[43] L. Guo, N. Jin, C. Gan, L. Xu, and Q. Wang, "An improved model predictive control strategy to reduce common-mode voltage for two-level voltage source inverters considering dead-time effects," *IEEE Trans. Ind. Electron.*, vol. 66, no. 5, pp. 3561–3572, May 2019.
[44] G. Tan, X. Wu, Z. Wang, and Z. Ye, "A generalized algorithm to eliminate spikes of common-mode voltages for CMVRPWM," *IEEE Trans. Power Electron.*, vol. 31, no. 9, pp. 6698–6709, Sep. 2016.
[45] X. Zhang, R. Burgos, D. Boroyevich, P. Mattavelli, and F. Wang, "Improved common-mode voltage elimination modulation with dead-time compensation for three-level neutral-point-clamped three-phase inverters," in *Proc. IEEE Energy Convers. Congr. Expo.*, 2013, pp. 4240–4246.
[46] N. Aizawa *et al.*, "Dead-time effect and its compensation in common-mode voltage elimination of PWM inverter with auxiliary inverter," in *Proc. Int. Power Electron. Conf.*, 2010, pp. 222–227.
[47] D. Han, "Conducted common mode electromagnetic interference in wide bandgap semiconductor devices based DC-fed motor drives: Challenges and solutions," M. S. thesis, Univ. Wisconsin-Madison, Madison, WI, USA, 2017.

Yang Huang (Student Member, IEEE) was born in Chongqing, China. He received the B.S. degree from Southeast University, Nanjing, China, in 2016, and the M.S. degree from the University of Michigan-Dearborn, Dearborn, MI, USA in 2018. He is currently working toward the Ph.D. degree in power electronics with the Department of Electrical Engineering and Computer Science, University of Tennessee-Knoxville, TN, USA.

His research interests include on-board EV charger and fast charger design, FPGA based controller design, motor drive techniques, and common-mode noise reduction.

Jared Walden (Student Member, IEEE) was born in Bowling Green, KY, USA. He received the B.S. degree in 2018 from Western Kentucky University, Bowling Green, KY, USA, and the master's degree from the Department of Electrical Engineering and Computer Science, University of Tennessee-Knoxville, Knoxville, TN, USA, in 2021.

He is a Power Electronics Engineer with Oak Ridge National Laboratory, Oak Ridge, TN, USA. His current research interests include WBG applications in power electronics and motor drives.

Ximu Zhang received the B.S. degree in electrical engineering from Xi'an Jiaotong University, Xi'an, China, in 2018, the M.S. degree in computer science from the University of Michigan-Dearborn, Dearborn, MI, USA, in 2019, and the M.S. degree in electrical engineering from the University of Tennessee-Knoxville, Knoxville, TN, USA, in 2021.

He is currently an AI Framework Engineer with Black Sesame Inc., San Jose, CA, USA.

Yu Yan (Student Member, IEEE) was born in Liaoning, China, in 1994. He received the B.S. and M.S. degrees in electrical engineering and automation from the Beijing Institute of Technology, Beijing, China, in 2016 and 2018, respectively. He is currently working toward the Ph.D. degree with the Department of Electrical and Computer Engineering, University of Tennessee, Knoxville, TN, USA.

His research interests include battery charger and PV system.

Hua Bai (Senior Member, IEEE) received the B.S. and Ph.D. degrees from the Department of Electrical Engineering, Tsinghua University, Beijing, China, in 2002 and 2007, respectively.

He was a Postdoctoral Fellow and a Research Scientist with the University of Michigan-Dearborn, Dearborn, MI, USA, in 2007 and 2009, respectively. From 2010 to 2016, he was an Assistant Professor with the Department of Electrical and Compurter Engineering, Kettering University. During 2017–2018, he was an Associate Professor with the University of Michigan-Dearborn. He is currently an Associate Professor of EECS, University of Tennessee, Knoxville, TN, USA. His research interests include power electronic modelling, control and integration including variable frequency motor drive system, high voltage and high power dc/dc converter, wide-bandgap devices, and hybrid electric vehicles.

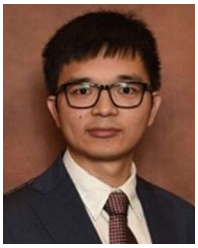

Fanning Jin (Student Member, IEEE) was born in China, in 1992. He received the B.E. degree in automation from the Huazhong University of Science and Technology, Hubei, China, in 2015, and the M.S.E. degree in electrical engineering from the University of Michigan-Dearborn, Dearborn, MI, USA, in 2017.

His research interests include field-programmable gate array utilization in various control algorithm (e.g., motor control) and hybrid energy storage system for EV applications.

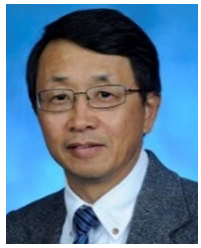

Bing Cheng (Member, IEEE) received the B.S. and M.S. degrees from Northeastern University, Shenyang, China, in 1982 and 1984, respectively, and the Ph.D. degree from the University of Massachusetts, Amherst, MA, USA, in 1992, all in electrical engineering.

From 1992 to 1994, he was with Cleveland Machine Controls, where he was responsible for ac induction motor control development for industrial drives. In 1994, he was with Ford Motor Company—Ecostar Electric Drives, LLC, which was acquired by Ballard Power Systems, Siemens VDO, and Continental Corporation. As a Principal Engineer, he performed research and development work on motor control software development, power electronic, and system simulation for fuel-cell and hybrid vehicles. From 2010 to 2015, he was the E-Motor Controls and Integration Manager with Fiat Chrysler Automobiles, Turin, Italy, where he was responsible for motor control, motor calibration, and software development for all the battery/hybrid electric vehicles programs. In 2015, he was a Motor Control and Calibration Manager with Mercedes-Benz Research and Development North America. He is currently responsible for E-drive motor control research and software development for hybrid and electric vehicle applications. Since 2013, he has been an Adjunct Professor with the Department Electrical Engineering, McMaster University, Hamilton, ON, Canada. His interests include control systems, electric machines, and power electronics in electric/hybrid vehicle applications.